Science Advances
AAAS

advances.sciencemag.org/cgi/content/full/5/2/eaau5999/DC1

Supplementary Materials for

Superadiabatic population transfer in a three-level superconducting circuit

Antti Vepsäläinen, Sergey Danilin, Gheorghe Sorin Paraoanu*

*Corresponding author. Email: sorin.paraoanu@aalto.fi

Published 8 February 2019, *Sci. Adv.* **5**, eaau5999 (2019)
DOI: 10.1126/sciadv.aau5999

This PDF file includes:

Experimental setup and sample

A transmon is an artificial atom with energy levels $\hbar\omega_j$, yielding transition frequencies $\omega_{j,j+1} = \omega_{j+1} - \omega_j$, and can be modelled as an anharmonic oscillator. With standard notations in the field of superconducting devices, we denote by E_J the Josephson energy of the transmon and by E_{C} the total charge energy (including the shunt capacitor). The anharmonicity is $\hbar\omega_{12} - \hbar\omega_{01} \approx -E_{\mathrm{C}}$ in the asymptotic limit $E_{\mathrm{J}} \gg E_{\mathrm{C}}$. To manipulate the state of the transmon we apply microwave drive signals either to the gate or to the coupled transmission line cavity. If the frequency of the drive matches the transition frequency between two states of the system, the system goes through Rabi oscillations, resulting in transfer of population between the two states.

The experimental setup including the schematic of the electronics used in this work is presented in fig. S1. The experiment was performed in a dilution refrigerator with base temperature below ~ 20 mK. The sample consists of a transmon coupled to a $\lambda/4$ - coplanar waveguide (CPW) resonator, and it is made of an aluminum film with 90 nm thickness, deposited on the surface of a silicon chip. The Josephson junctions of the transmon are realized by the shadow deposition technique, and have roughly an area of 220×260 nm^2. The transition frequencies

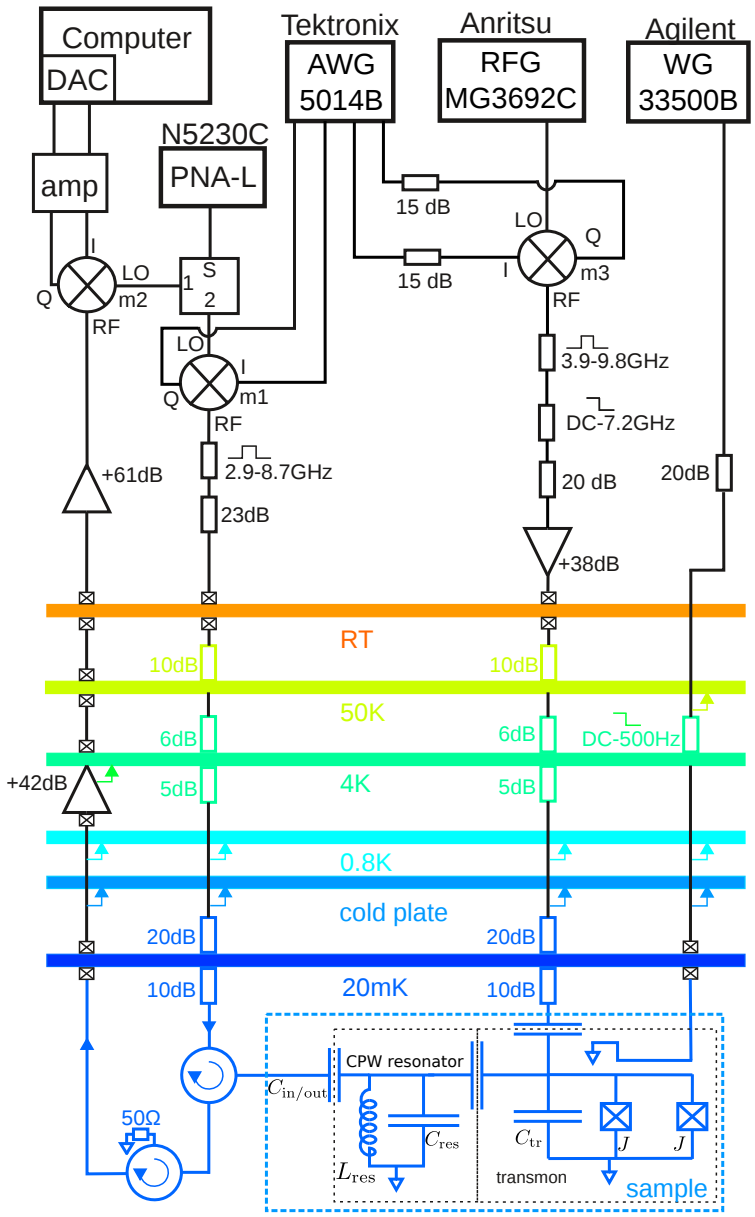

Fig. S1. **Electronics, cryogenics, and sample schematic.** The sample consists of a transmon device coupled to $\lambda/4$ coplanar waveguide resonator. It is placed at the mixing chamber of a dilution refrigerator and controlled by room-temperature electronics.

of the transmon can be tuned by varying the magnetic flux threading the SQUID loop of the device, which is done by changing the current flowing through a nearby line, see fig. S1. The

microwave pulses to control the transmon state are sent to the gate line, which is capacitively coupled to the transmon. The charging energy of the transmon $E_C \simeq h \cdot 370$ MHz and its maximum Josephson energy $E_{J\Sigma} = E_{J,1} + E_{J,2} \simeq 17.94$ GHz (with nearly identical Josephson junctions) were determined by spectroscopy measurements. The resonant frequency of the resonator, when the transmon is far detuned from it, was $f_r \simeq 5.126$ GHz with the loaded quality factor $Q \simeq 3400$. The vacuum Rabi coupling strength between the transmon and the resonator $g \simeq 41$ MHz was determined from the avoided crossing observed when the resonator and the transmon frequencies are close to each other.

Due to the coupling between the transmon and the coplanar waveguide (CPW) resonator, the state of the former is encoded into the resonant frequency of the latter, so the state of the transmon can be deduced by sending a microwave probe pulse to the resonator and measuring the reflected signal. A homodyne detection scheme was used to achieve this. The continuous microwave at frequency $f_p = 5.126$ GHz, provided by a vector network analyzer (PNA-L N5230C) is split into two parts: the first of them is shaped into a probe rectangular pulse with the use of an IQ-mixer (IQ-0307LXP, m1 in fig. S1), while the second part serves as a LO signal for the detection part of the scheme. The reflected signal was demodulated with the same type of IQ-mixer (denoted by m2) and recorded with a high speed ADC (Acquiris U1082a).

An Agilent 33500B waveform generator was employed to provide a DC voltage to the flux bias line used to generate the magnetic flux piercing the transmon SQUID loop. To reduce the flux noise this voltage was filtered with a passive low pass RC-filter placed at the 4K-flange of the cryostat, with cut-off frequency of ~ 500 Hz. A key element in the setup was the mixer denoted by m3 (see fig. S1), which was used to generate the microwave gate pulses for state manipulation. To do this, two channels from a Tektronix 5014B arbitrary waveform generator (AWG) were used to input modulated IF waves, and a microwave signal generator (Anritsu MG3692C) provided the local oscillator (LO) signal. The IF waves were programmed

in the waveform generator: their frequency was such that, after mixing, they would match the frequencies of the corresponding transmon transitions. The LO leakeage in this mixer was compensated by additional dc bias voltages applied to the ports, and reduced down to the level of the background noise. As a result of frequency mixing, in addition to the desired signal at the frequency LO $-$ IF, a mirror image appears at the frequency LO $+$ IF, which, if left uncorrected, could produce spurious excitations to higher levels. We employed standard single-sideband (SSB) calibration by adding the same IF waveform as that applied to the I port into the Q port of the IQ-mixer, but with the phase shifted by $\pi/2$. The output signal from the mixer was filtered and then amplified in order to be able to achieve Rabi oscillations with short duration pulses.

The dependence of the 0 – 1 transition frequency on flux was determined from spectroscopy measurements, where one microwave tone was sent to the resonator, and another tone was used to excite the qutrit. By increasing the qutrit excitation tone power we could also identify the two-photon transition frequency to the second excited state. The π pulses for all three transitions (0 – 1, 0 – 2, and 1 – 2) were extracted from standard Rabi experiments. The relaxation rate $\Gamma_{01} = 0.6$ MHz was determined by first exciting the transmon to the state $|1\rangle$ with a π pulse and recording the exponential decay traces to the state $|0\rangle$ as a function of time. To find the rate $\Gamma_{21} = 0.83$ MHz we excited the transmon to state $|2\rangle$ with a two-photon π pulse and observed its decay to the ground state. Γ_{21} was found by fitting the numerical three-level exponential decay model to the measured data. Additional sources of noise exist in the experimental setup, which lead to energy level shifts and dephasing. The pure dephasing rates of the 01 and 12 transitions were determined from the Ramsey experiment to be $\Gamma_\phi^{01} \approx \Gamma_\phi^{12} \approx 0.09$ MHz. Consequently, for this particular sample the relaxation rates provide the dominant decoherence mechanism.

Using this arrangement, we were able to generate the three overlapping gate pulses needed for the experiment. The two STIRAP pulses were resonant with the 0 - 1 and 1- 2 transitions of the transmon, at frequencies ω_{01} and ω_{12}. The third pulse was used to drive the two-photon 0 -

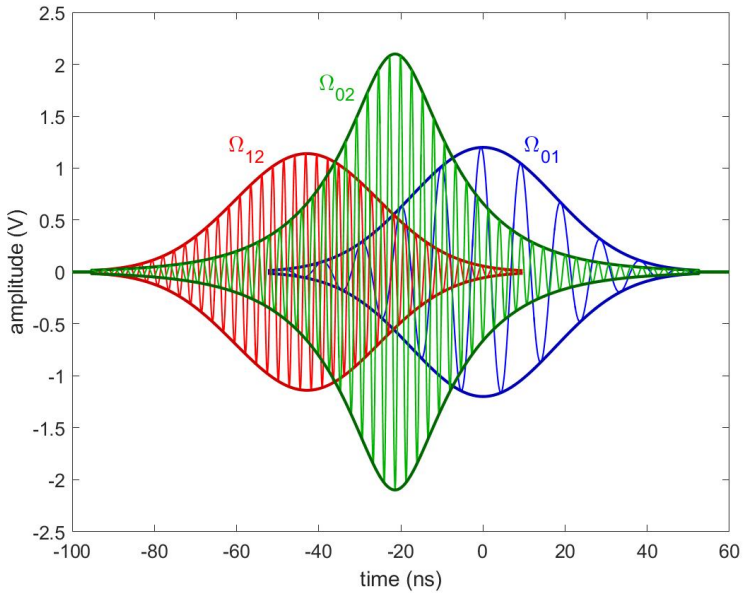

Fig. S2. **Pulse sequence for saSTIRAP.** The qutrit is controlled by three microwave pulses applied to the transitions $0-1$, $1-2$, and $0-2$. The pulses are created by an arbitrary waveform generator, leading to the corresponding Rabi couplings Ω_{01}, Ω_{12}, and Ω_{02}.

2 transition and had the frequency $\omega_{02} = (\omega_{01} + \omega_{12})/2$. Thus, by programming the following wavefunctions

$$A_{01}(t) = A_{01} \exp\left(-\frac{t^2}{2\sigma^2}\right) \times \sin(\mathrm{IF}_{01} t + \phi_{01}), \tag{1}$$

$$A_{12}(t) = A_{12} \exp\left[-\frac{(t-t_\mathrm{s})^2}{2\sigma^2}\right] \times \sin(\mathrm{IF}_{12} t + \phi_{12}), \quad \text{and} \tag{2}$$

$$A_{2\mathrm{ph}}(t) = A_{2\mathrm{ph}} \frac{1}{\sqrt{\cosh\left[\frac{t_\mathrm{s}(t-t_\mathrm{s}/2)}{\sigma^2}\right]}} \times \sin(\mathrm{IF}_{02} t + \phi_{2\mathrm{ph}}) \tag{3}$$

into the Tektronix arbitrary waveform generator, we were able to drive the transmon with tones at ω_{01}, ω_{12}, ω_{02}, and with the pulse envelopes required by the saSTIRAP protocol. Here the coefficients A_{01}, A_{12}, and $A_{2\mathrm{ph}}$ are the amplitudes of the IF pulses in volts.

The LO frequency (common to all three pulses) was LO = $2\pi \times 6.92$ GHz. The LO frequency was chosen to be sufficiently far away from all the transition frequencies to reduce even more

the probability of spurious excitations. From this, we obtained the desired pulses by applying amplitude modulated waveforms to the I and Q ports of the IQ-mixer m3 with the following IF modulation frequencies

$$\mathrm{IF}_{01} = \mathrm{LO} - \omega_{01}, \qquad \mathrm{IF}_{12} = \mathrm{LO} - \omega_{12}, \qquad \mathrm{IF}_{02} = \mathrm{LO} - \omega_{02} \tag{4}$$

The first two pulses are Gaussian shaped with standard deviation σ, and they produce the Ω_{01} and Ω_{12} drives (blue and red in fig. S2) when coupled into the corresponding transitions of the transmon. The third pulse Ω_{02} (green in fig. S2) has a special shape: its maximum lays in-between the Ω_{01} and Ω_{12} pulses, and it has a phase shift $\phi_{2\mathrm{ph}}$ with respect to the Gaussian pulses. The Ω_{01} and Ω_{12} pulses were truncated at $\pm 3\sigma$ from their maxima. To ensure overlap with the STIRAP pulses irrespective to the time delay t_s, the truncation of the two-photon pulse is performed in such a way that it is zero only when both of the pulses Ω_{01} or Ω_{12} are zero (see fig. S2).

The voltages $A_{i,j}$ were converted to Rabi rates $\Omega_{i,j}$ using a calibration experiment, where the pulse amplitude is increased until a full π-pulse is created. The experiment is repeated for the 0–1, 1–2 and 0–2 transitions.

An important observation is that once the phase difference between the two-photon pulse and the sum of the STIRAP phases is fixed at some reference time $t^{[\mathrm{ref}]}$, it will remain the same at any further moment in time. Suppose that the phase of the counterdiabatic two-photon pulse is $\phi_{2\mathrm{ph}}^{[\mathrm{ref}]}$, while those of the STIRAP pulses are $\phi_{01}^{[\mathrm{ref}]}$ and $\phi_{12}^{[\mathrm{ref}]}$ at a time $t^{[\mathrm{ref}]}$; then at a later time t the two-photon phase has advanced to $2\omega_{02}(t - t^{[\mathrm{ref}]}) + 2\phi_{2\mathrm{ph}}^{[\mathrm{ref}]}$, while the total STIRAP phase to $\omega_{01}(t - t^{[\mathrm{ref}])}) + \phi_{01}^{[\mathrm{ref}]} + \omega_{12}(t - t^{[\mathrm{ref}]}) + \phi_{12}^{[\mathrm{ref}]}$. The difference between these two quantities is therefore time-independent, since $2\omega_{02} = \omega_{01} + \omega_{12}$.

The two photon driving creates small ac Stark shifts in the energy levels of the qutrit. To compensate for these, a dynamical phase correction was introduced to the drive envelopes by

adding an additional phase factor $\tilde{\phi}_{ij}(t)$, as described in Methods. The corrected pulse shapes are

$$\tilde{A}_{01}(t) = A_{01} \exp\left(-\frac{t^2}{2\sigma^2}\right) \times \sin[\mathrm{IF}_{01} t + \phi_{01} + \tilde{\phi}_{01}(t)], \tag{5}$$

$$\tilde{A}_{12}(t) = A_{12} \exp\left[-\frac{(t-t_\mathrm{s})^2}{2\sigma^2}\right] \times \sin[\mathrm{IF}_{12} t + \phi_{12} + \tilde{\phi}_{12}(t)], \quad \text{and} \tag{6}$$

$$\tilde{A}_{2\mathrm{ph}}(t) = A_{2\mathrm{ph}} \frac{1}{\sqrt{\cosh\left[\frac{t_\mathrm{s}(t-t_\mathrm{s}/2)}{\sigma^2}\right]}} \times \sin[\mathrm{IF}_{02} t + \phi_{2\mathrm{ph}} + \tilde{\phi}_{02}(t)/2] \tag{7}$$

where $\tilde{\phi}_{ij} = \int_{-\infty}^{t} \mathrm{d}t \epsilon_{ij}(t)/\hbar$ as given in the main text. Note that the phase correction coefficient $\tilde{\phi}_{02}(t)$ is divided by 2 due to the two-photon driving.

As always in experiments, the devices used for control and measurement are imperfect, and as a result deviations from the ideal case occur. Due to the finite bandwidth of the Tektronix waveform generator, the IF signals are only approximately given by the expressions Eq. 5 - 7. Next along the control line, the single sideband cancellation procedure for the mixer m3 introduces also a phase shift ϕ^ϵ in the resulting tone at the RF output. This phase shift is frequency-dependent and therefore it will be different for each of the three IF waveforms. The end result is that the gauge-invariant Φ will acquire a constant phase error $\phi^\epsilon_{01} + \phi^\epsilon_{12} - 2\phi^\epsilon_{2\mathrm{ph}}$. This shows up as a phase shift in Fig. 5 in the main text. Next, as the signal reaches the sample, the bonding wires have a finite inductance, resulting in mismatching to the 50 Ohms line impedance and therefore in slight deformations of the pulses as seen by the transmom.

Reverse engineering of the counteradiabatic drive

For completeness we give here a systematic derivation of the method used to find the counter-diabatic drive Hamiltonian H_cd. For reference, see *e.g.* (*19, 35*). Given a Hamiltonian

$$H_0(t) = \sum_n \lambda_n(t) |n(t)\rangle\langle n(t)| \tag{8}$$

where $|n(t)\rangle$ are the eigenvectors and $\lambda_n(t)$ are the eigenvalues, the exact solution of the Schrödinger equation $i\hbar\partial_t|\psi(t)\rangle = H_0(t)|\psi(t)\rangle$ can be obtained by expanding the wavefunction into the instantaneous eigenstates $|n(t)\rangle$

$$|\psi(t)\rangle = \sum_n c_n e^{i\zeta_n(t)}|n(t)\rangle \tag{9}$$

Using this expansion, as well as the identity

$$\langle n|\partial_t m\rangle = \frac{\langle n|(\partial_t H_0)|m\rangle}{\lambda_m - \lambda_n} \tag{10}$$

obtained from taking the time derivative of $H_0|m\rangle = \lambda_m|m\rangle$, we get

$$\dot{c}_n + i\dot{\zeta}_n c_n + c_n\langle n|\partial_t n\rangle + \frac{i}{\hbar}\lambda_n c_n + \sum_{m\neq n} c_m \frac{\langle n|(\partial_t H_0)|m\rangle}{\lambda_m - \lambda_n} e^{i(\zeta_m - \zeta_n)} = 0 \tag{11}$$

The adiabatic theorem (*45*) allows us to neglect the last term of the left hand side. Therefore in this approximation the system remains (up to a phase) in the state $|n(t)\rangle$ if it started in $|n(0)\rangle$ and there are no transitions on states $m \neq n$ during the evolution. Therefore, without loss of generality, we can take $c_n = 1$, and obtain the equation for the phase

$$\dot{\zeta}_n(t) = -\frac{1}{\hbar}\lambda_n(t) + i\langle n(t)|\partial_t n(t)\rangle \tag{12}$$

which can be integrated immediately to find $\zeta(t)$ at any time t. Note that $\zeta(t)$ comprises a dynamical component $-\int_0^t d\tau\lambda_n(\tau)/\hbar$ as well as a geometric (Berry) phase part $i\int_0^t d\tau\langle n(\tau)|\partial_\tau n(\tau)\rangle$. Thus, in the adiabatic approximation the state of the system at any time t, starting in an eigenstate $|n(0)\rangle$ is

$$|\psi(t)\rangle_{\rm ad} = e^{i\zeta_n(t)}|n(t)\rangle \tag{13}$$

with the phase given by the solution of Eq.12.

Now, we would like to design a total Hamiltonian $H(t)$ such that the evolution of the system under its action follows exactly the approximate adiabatic solution of Eq.13. The unitary evolution

operator which would take the system along $|\psi(t)\rangle_{\rm ad}$ is

$$U(t) = \sum_n e^{i\zeta_n(t)} |n(t)\rangle\langle n(0)| \tag{14}$$

This can be implemented by reverse-engineering the evolution – that is, given the unitary Eq. 14 we would like to find a Hamiltonian $H(t)$ such that

$$i\hbar\dot{U}(t) = H(t)U(t) \tag{15}$$

The formal solution for $H(t)$, from the equation above, is

$$H(t) = i\hbar\dot{U}(t)U^\dagger(t) \tag{16}$$

Using now Eqs. 12 and 14 we find that

$$H(t) = H_0(t) + H_{\rm cd}(t) \tag{17}$$

and now we are able to identify the counteradiabatic drive Hamiltonian as

$$H_{\rm cd}(t) = i\hbar \sum_n [|\partial_t n(t)\rangle\langle n(t)| - \langle n(t)|\partial_t n(t)\rangle |n(t)\rangle\langle n(t)|] \tag{18}$$

In the adiabatic basis, the drive Hamiltonian has only off-diagonal elements ($\langle n(t)|H_{\rm d}(t)|n(t)\rangle = 0$) which can be expressed using Eq. 10 as

$$\langle m(t)|H_{\rm cd}(t)|n(t)\rangle|_{n\neq m} = i\hbar \frac{\langle m(t)|(\partial_t H_0)|n(t)\rangle}{\lambda_n(t) - \lambda_m(t)} \tag{19}$$

We now apply this general result to the three-level system, with energy eigenstates $|0\rangle$, $|1\rangle$, and $|2\rangle$, driven resonantly by the two fields with frequencies ω_{01} and ω_{12}, which couple into the transitions $|0\rangle \rightarrow |1\rangle$ and $|1\rangle \rightarrow |2\rangle$ with Rabi frequencies $\Omega_{01}(t)$ (pump) respectively $\Omega_{12}(t)$ (Stokes). In the rotating wave approximation with respect to the two tones, the effective three-level Hamiltonian takes the form (*8, 32, 46, 47*)

$$H_0(t) = \frac{\hbar}{2}\begin{bmatrix} 0 & \Omega_{01}(t) & 0 \\ \Omega_{01}(t) & 0 & \Omega_{12}(t) \\ 0 & \Omega_{12}(t) & 0 \end{bmatrix} \tag{20}$$

For simplicity we have taken here the Rabi couplings $\Omega_{01}(t)$ and $\Omega_{12}(t)$ to be real. Using the standard parametrization of the relative strengths of the pump and Stokes frequencies by an angle Θ

$$\tan\Theta(t) = \frac{\Omega_{01}(t)}{\Omega_{12}(t)} \tag{21}$$

we can express the eigenvectors of this Hamiltonian as

$$\begin{aligned} |n_+(t)\rangle &= \frac{1}{\sqrt{2}}\sin\Theta(t)|0\rangle + \frac{1}{\sqrt{2}}|1\rangle + \frac{1}{\sqrt{2}}\cos\Theta(t)|2\rangle, \\ |n_-(t)\rangle &= \frac{1}{\sqrt{2}}\sin\Theta(t)|0\rangle - \frac{1}{\sqrt{2}}|1\rangle + \frac{1}{\sqrt{2}}\cos\Theta(t)|2\rangle, \\ |n_0(t)\rangle &= \cos\Theta(t)|0\rangle - \sin\Theta(t)|2\rangle \end{aligned} \tag{22}$$

and corresponding eigenvalues

$$\begin{aligned} \lambda_+(t) &= \frac{\hbar}{2}\sqrt{\Omega_{01}^2(t) + \Omega_{12}^2(t)}, \\ \lambda_-(t) &= -\frac{\hbar}{2}\sqrt{\Omega_{01}^2(t) + \Omega_{12}^2(t)}, \\ \lambda_0(t) &= 0 \end{aligned} \tag{23}$$

The last eigenvector is a dark state.

Now, to identify the driving Hamiltonian, we plug in the expression for eigenvectors in Eq. 22 into Eq. 18. After some algebraic calculations and noticing that the terms $\langle n(t)|\partial_t n(t)\rangle$ are all zero, we obtain a remarkably simple result

$$H_{\rm cd}(t) = \frac{\hbar}{2}\begin{bmatrix} 0 & 0 & \Omega_{02}(t)e^{i\pi/2} \\ 0 & 0 & 0 \\ \Omega_{02}(t)e^{-i\pi/2} & 0 & 0 \end{bmatrix} \tag{24}$$

where $\Omega_{02}(t) = 2\dot{\Theta}(t)$. Integrating the absolute value of $\Omega_{\rm cd}(t)$ between an initial time $t_{\rm in}$ and a final time $t_{\rm fin}$ we get the pulse area condition

$$\int_{t_{\rm in}}^{t_{\rm fin}} |\Omega_{\rm cd}(t')|dt' = 2\Theta(t_{\rm fin}) - 2\Theta(t_{\rm in}) \tag{25}$$

Thus, if the drive Hamiltonian is intended to correct a full STIRAP, for which $\Theta(t_{\rm in}) = 0$ and $\Theta(t_{\rm fin}) = \pi/2$, a total area of π is needed for the counterdrive pulse. Note also that the quantum control implemented by Eq. 24 – or in general by Eq. 18 – implements a standard linear evolution and it is also state-independent.

In the experiment the pump and Stokes pulses of the STIRAP protocol are Gaussians of equal width σ delayed with respect to each other by a separation time $t_{\rm s}$

$$\Omega_{01}(t) = \Omega_{01} \exp\left[-\frac{t^2}{2\sigma^2}\right], \tag{26}$$

$$\Omega_{12}(t) = \Omega_{12} \exp\left[-\frac{(t-t_s)^2}{2\sigma^2}\right] \tag{27}$$

where time is measured from the maximum of the $0-1$ pulse. In this convention, STIRAP is realized at negative times $t_{\rm s}$, while the intuitive sequence corresponds to positive $t_{\rm s}$

From Eq. 21 we obtain

$$\dot{\Theta}(t) = \frac{\dot{\Omega}_{01}(t)\Omega_{12}(t) - \Omega_{01}(t)\dot{\Omega}_{12}(t)}{\Omega_{01}^2(t) + \Omega_{12}^2(t)} \tag{28}$$

In the case $\Omega_{01} = \Omega_{12}$ we get

$$\dot{\Theta}(t) = -\frac{t_{\rm s}}{2\sigma^2} \sin\left[2\Theta(t)\right] \tag{29}$$

or

$$\dot{\Theta} = -\frac{t_{\rm s}}{2\sigma^2} \frac{1}{\cosh\left[\frac{t_{\rm s}}{\sigma^2}\left(t - \frac{t_{\rm s}}{2}\right)\right]} \tag{30}$$

Furthermore, in this simple all-resonant configuration it is straigthforward to derive the local adiabaticity condition for the STIRAP pulses (valid for any pulse shape), which reads

$$|\dot{\Theta}(t)| \ll \sqrt{\Omega_{01}^2(t) + \Omega_{12}^2(t)} \tag{31}$$

Retaining the nonadiabatic terms in Eq. 11, with the solution Eq. 12 and the substitution $c_{\pm}(t) = \tilde{c}_{\pm}(t) \exp\left[-\frac{1}{\hbar}\int_0^t dt' \lambda_{\pm}(t')\right]$ (thus separating the trivial dynamical evolution from

the adiabatic one), we obtain

$$\begin{aligned}
\dot{c}_0(t) &= -\frac{\dot{\Theta}(t)}{\sqrt{2}}\tilde{c}_+(t) - \frac{\dot{\Theta}(t)}{\sqrt{2}}\tilde{c}_-(t), \\
\dot{\tilde{c}}_+(t) &= -\frac{i}{2}\sqrt{\Omega_{01}^2(t) + \Omega_{12}^2(t)}\tilde{c}_+(t) - \frac{\dot{\Theta}(t)}{\sqrt{2}}c_0(t), \\
\dot{\tilde{c}}_-(t) &= \frac{i}{2}\sqrt{\Omega_{01}^2(t) + \Omega_{12}^2(t)}\tilde{c}_+(t) - \frac{\dot{\Theta}(t)}{\sqrt{2}}c_0(t)
\end{aligned} \tag{32}$$

Thus the condition in Eq. 31 ensures that there are no transitions between the instantaneous adiabatic states during the evolution.

Synthetic Peierls couplings on the triangular plaquette

The loop driving configuration used in the experiment produces a nontrivial gauge structure, as shown in the schematic of Fig. 1 d) in the main text. In this picture, the internal states of the transmon can be regarded as sites in a synthetic dimension (*41*).

To explore this concept in detail, we adapt some of the results obtained earlier in (*36*) to our setup. Consider what happens under local U(1) transformations with phases χ_0, χ_1, and χ_2 on each of the three states. The unitary that achieves this is

$$U = e^{-i\chi_0}|0\rangle\langle 0| + e^{-i\chi_1}|1\rangle\langle 1| + e^{-i\chi_2}|2\rangle\langle 2| \tag{33}$$

leading to a transformed Hamiltonian $H' = UHU^\dagger$ and

$$H' = \frac{\hbar}{2}\Omega_{01}e^{i\phi'_{01}}|0\rangle\langle 1| + \frac{\hbar}{2}\Omega_{12}e^{i\phi'_{12}}|1\rangle\langle 2| + \frac{\hbar}{2}\Omega_{02}e^{i\phi'_{02}}|0\rangle\langle 2| + \text{h.c.} \tag{34}$$

The equations for the phases χ_0, χ_1, and χ_2 are

$$\begin{bmatrix} -1 & 1 & 0 \\ 0 & -1 & 1 \\ 1 & 0 & -1 \end{bmatrix} \begin{bmatrix} \chi_0 \\ \chi_1 \\ \chi_2 \end{bmatrix} = \begin{bmatrix} \phi'_{01} - \phi_{01} \\ \phi'_{12} - \phi_{12} \\ \phi'_{20} - \phi_{20} \end{bmatrix} \tag{35}$$

Here, to put in evidence the circularity under the permutation of indices 0, 1, and 2, we have replaced $\phi_{02} = -\phi_{20}$, and $\phi'_{02} = -\phi'_{20}$. A first observation is that the 3×3 matrix appearing

in the equation above is singular. Given a choice of desired phases ϕ'_{01}, ϕ'_{12}, and ϕ'_{20}, because the matrix is not invertible, we are not guaranteed that we can find the local gauge phases χ_0, χ_1, and χ_2 such that the form H' is obtained. Indeed, by adding up the three equations from the matrix form in Eq. 35 we obtain the constraint that the sum of the phases ϕ_{ij} (in the circular order for the indices i, j) before and after the transformation must be the same

$$\Phi = \phi'_{01} + \phi'_{12} + \phi'_{20} = \phi_{01} + \phi_{12} + \phi_{20} \tag{36}$$

This constraint implies that we cannot eliminate all three phases simultaneously, and it results from the existence, in the loop driving configuration, of three nonzero Rabi frequencies Ω_{01}, Ω_{12}, and Ω_{02}. If any one of these Rabi frequencies would be zero, the phase elimination could be done. Suppose for example that $\Omega_{02} = 0$. In this case we can obtain the Hamiltonian (34) with all the elements real, by choosing for example $\chi_0 = 0$, $\chi_1 = -\phi_{01}$, and $\chi_2 = -\phi_{01} - \phi_{12}$. However, if $\Omega_{02} \neq 0$, then the same choice of gauges leads to $\phi'_{01} = \phi'_{12} = 0$ and $\phi_{20} = \Phi$. From an experimental point of view the existence of this constraint provides us with a useful "knob" for controlling the system, through adjustments of the phase Φ. By arranging χ_0, χ_1, χ_2 such that $\phi'_{01} = \phi'_{12} = 0$ we get a convenient final form for the Hamiltonian

$$H = \frac{\hbar}{2}|0\rangle\langle 1| + \frac{\hbar}{2}\Omega_{12}|1\rangle\langle 2| + \frac{\hbar}{2}\Omega_{02}e^{-i\Phi}|0\rangle\langle 2| + \text{h.c.} \tag{37}$$

In this gauge, the STIRAP part is $H_0 = (\hbar/2)\Omega_{01}|0\rangle\langle 1| + (\hbar/2)\Omega_{12}|1\rangle\langle 2| + \text{h.c.}$, while the counterdiabatic part needed for saSTIRAP is realized at $\Phi = -\pi/2$ and it takes the familiar form $H_{\text{cd}} = i(\hbar/2)\Omega_{02}(t)|0\rangle\langle 2| + \text{h.c.}$ (*35*). Seen as an Aharonov-Bohm effect, this situation corresponds to constructive interference on the state $|2\rangle$ between the direct two-photon drive and the STIRAP process.

Finally, one notices that Eq. 35, which defines the change in the gauge, is the discrete-space analogous of the well-known relation $\vec{A}' = \vec{A} + \nabla\chi$, which describes a change of gauge for the vector magnetic field, written for a lattice with 3 positions corresponding to the "localized"

states $|0\rangle$, $|1\rangle$, and $|2\rangle$. The differences $\chi_1 \ -\chi_0$,$\chi_2 \ -\chi_1$,and $\chi_0 - \chi_2$ which appear in Eq. 35 are the discrete version of the continuous space derivative $\nabla\chi$. The sum of the phases Φ is the discrete version of the line integral $\oint \vec{A}\mathrm{d}\vec{l}$, which is the magnetic flux penetrating the plaquette formed by the three sites.

To make this more precise, let us define a lattice gauge Hamiltonian model: a spinless particle that can jump between three sites, 0,1, and 2. In the second order quantization, the states with one particle at the site 0, 1, or 2 can be written respectively as $|1,0,0\rangle$, $|0,1,0\rangle$, and $|0,0,1\rangle$. Formally, we can identify these states with the standard qutrit basis $|0\rangle, |1\rangle, |2\rangle$

$$|1,0,0\rangle \equiv |0\rangle, |0,1,0\rangle \equiv |1\rangle, |0,0,1\rangle \equiv |2\rangle \tag{38}$$

Then the Hamiltonian takes the form

$$H = \frac{\hbar}{2} \sum_{<j,k>} \Omega_{jk} e^{i\phi_{jk}} c_j^\dagger c_k \tag{39}$$

with the convention $\phi_{jk} = -\phi_{kj}$. As usual in lattice field theory, the complex factors

$$U_{jk} = U_{kj}^* = e^{i\phi_{jk}} \in U(1) \tag{40}$$

are referred to as link variables (Peierls phases). Then the Aharonov-Bohm phase accumulated due to transport across the plaquette (loop) is

$$e^{i\Phi} = \prod_{\triangle} U_{jk} = U_{01}U_{12}U_{20} = e^{i(\phi_{01}+\phi_{12}+\phi_{20})} \tag{41}$$

where the product is taken in circular order. Now, we can introduce a gauge potential $\mathcal{A}$ in the standard way, such that the integral of this quantity between two points j and k equals the phase ϕ_{jk}

$$\phi_{jk} = \frac{1}{\hbar} \int_j^k \mathcal{A} d\mathbf{l} \tag{42}$$

Thus, we consider that the gauge field $\mathcal{A}$ is defined along the links that connect the sites. If this gauge field is produced by a standard magnetic field piercing the plaquette, then $\mathcal{A} = qA$, where q is the charge, and $\frac{1}{\hbar}\int_j^k \mathcal{A}d\mathbf{l}$ is referred to as magnetic phase factor.

Then, we define a gauge transformation $A \to A' = A + \nabla\chi$. This changes the link variables as

$$U_{jk} \to U'_{jk} = e^{\frac{i}{\hbar}(\chi_k - \chi_j)} U_{jk} \tag{43}$$

resulting for the entire loop in

$$e^{i\Phi'} = \prod_{\triangle} U'_{jk} = e^{\sum_{\triangle} \frac{i}{\hbar}(\chi_k - \chi_j)} \prod_{\triangle} U_{jk} = \prod_{\triangle} U_{jk} = e^{i\Phi} \tag{44}$$

Here the indices are summed in circular order. Thus, Φ is gauge invariant, and via Stoke's theorem $\oint A d\mathbf{l} = \int\int B d\mathbf{s}$. If the gauge field is the magnetic vector potential, $A = q\mathbf{A}$, then $\mathbf{B} = \nabla \times A$ is the magnetic field and

$$\Phi = 2\pi \frac{q}{h} \int\int \mathbf{B} d\mathbf{s} \tag{45}$$

is 2π times the magnetic flux expressed in units of flux quanta h/q.